Aberystwyth University

A Monte Carlo error analysis for basal sliding velocity calculations

D. M. Chandler,[1] A. L. Hubbard,[2] B. P. Hubbard,[1] and P. W. Nienow[2]

[1] Since glacier beds are mostly inaccessible, numerical inversion of the surface velocity field provides a valuable method for calculating the basal shear stress and sliding velocity. However, previous theoretical studies (limited either to planar slabs or linear ice rheology) have suggested small errors in surface velocity measurements lead to large uncertainties in calculated basal sliding. Here a numerical ice flow model and Monte Carlo simulation are used to calculate the sliding velocity and basal shear stress and their associated uncertainties from field measurements of surface velocity along a two-dimensional long section of Glacier de Tsanfleuron, Switzerland. The model does not require the restrictive assumption of a sliding law since both sliding and basal shear stress are calculated independently and can include a spatially variable rate factor in the flow law for ice. Results indicate that sliding contributes between 45 and 84% of the surface velocity and that calculated sliding velocities are strongly dependent on ice rheology. Amplification of surface velocity errors is generally smaller than theoretical estimates and is a power law function of the horizontal grid spacing in the ice flow model.

Citation: Chandler, D. M., A. L. Hubbard, B. P. Hubbard, and P. W. Nienow (2006), A Monte Carlo error analysis for basal sliding velocity calculations, *J. Geophys. Res.*, *111*, F04005, doi:10.1029/2006JF000476.

1. Introduction

[2] Many field techniques have been developed to measure the basal sliding rate of glaciers, either by direct instrumentation at the bed [e.g., *Haefeli*, 1951; *Harrison and Kamb*, 1970; *Vivian*, 1971; *Blake et al.*, 1994; *Cohen et al.*, 2000; *Hubbard*, 2002] or indirectly via borehole deformation measurements [e.g., *Gerrard et al.*, 1952; *Raymond*, 1971; *Hooke et al.*, 1987, 1992; *Harbor et al.*, 1997; *Harper et al.*, 1998; *Gudmundsson et al.*, 1999]. While these methods allow measurements or estimates of the local sliding velocity, the resulting data are limited to a small number of specific locations and are not necessarily representative of the full range of subglacial conditions.

[3] As an alternative to direct measurements, analysis of surface velocity variations in space or time can provide estimates of the sliding velocity field. In this case no subglacial access is required and data on surface geometry and velocity are becoming more widely available with advances in remote sensing. Estimates of sliding rate have been made using diurnal or seasonal variations in surface motion under the assumption that temporary increases in surface velocity are due to increases in sliding [e.g., *Bindschadler et al.*, 1977; *Bindschadler*, 1983; *Hubbard et al.*, 1998]. While variations in surface motion have been found with little or no change in internal deforma-

tion rate [*Harper et al.*, 1998], sliding estimates using this method will be too small if sliding still occurs during low-velocity periods, and estimated variations in sliding are subject to uncertainty if internal deformation rates also vary during peak surface velocities, such as at Storglaciären, Sweden [*Hooke et al.*, 1992] and Lauteraargletscher, Switzerland [*Sugiyama et al.*, 2003]. Reduction of uncertainties arising from varying internal strain rates can be achieved by numerically modeling the ice flow [e.g., *Fastook et al.*, 1995; *Hanson*, 1995; *Le Meur and Vincent*, 2003; *Thorsteinsson et al.*, 2003]. In these studies, a sliding law is usually assumed and is typically of the form

$$u_0 = k \tau_b^a N^{-b} \tag{1}$$

where u_0 is the sliding velocity, τ_b is the basal shear stress and N is the effective pressure (ice overburden pressure minus the subglacial water pressure). The coefficient k is likely to depend on several controls, for example bed roughness, and has been treated as a constant [*Hanson*, 1995; *Le Meur and Vincent*, 2003] or, probably more realistically, as a variable [*Harbor*, 1992; *Thorsteinsson et al.*, 2003]. There are no standard values for a, b and k in equation (1) and some or all of these parameters, along with the rate factor in the ice flow law (see below), can be used as tuning parameters to match model output to field measurements. Typically $1 \leq a \leq 3$ and, if N is included, $b = 1$ [e.g., *Bindschadler*, 1983; *Harbor*, 1992; *Fastook et al.*, 1995; *Le Meur and Vincent*, 2003]. Dependence of these studies on the validity of equation (1) is a major drawback to this approach.

[4] Sliding velocities can be calculated without the restrictive assumptions that accompany the application of a sliding law. The simplest solution, if longitudinal stresses

---

[1]Centre for Glaciology, Institute of Geography and Earth Sciences, University of Wales, Aberystwyth, UK.

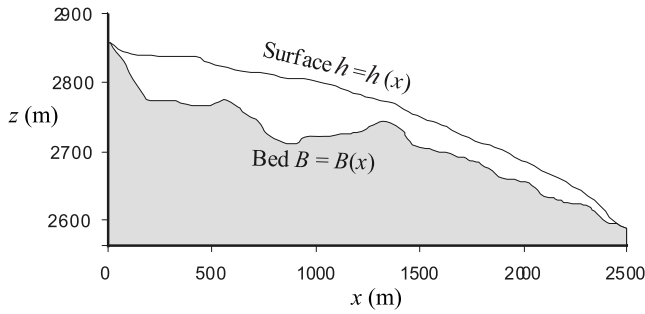[2]School of Geosciences, University of Edinburgh, Edinburgh, UK.

Figure 1. Glacier geometry used in the 2-D ice flow model.

are ignored, is to calculate sliding (or sliding plus bed deformation) by subtracting the estimated internal deformation component from measured surface velocities [e.g., *Hodge*, 1974]. To account for longitudinal stresses, which can be of a similar order of magnitude to the driving stress in valley glaciers [*Hubbard*, 2000], *Van der Veen and Whillans* [1989] developed an algorithm in which the ice flow equations were numerically integrated downward from the surface to the bed to calculate basal traction and basal sliding. However, downward integration is numerically unstable and can lead to artifacts in calculated basal stress and velocity fields [*Bahr et al.*, 1994; *Lliboutry*, 1995]. To overcome this problem, *Truffer* [2004] applied geophysical inverse theory in which the measured and modeled surface data are fitted to within a given tolerance. *Truffer*'s [2004] one-dimensional (1-D) forward model is based on the shallow ice approximation (SIA) for ice flow in a confined channel, with a correction factor for longitudinal variations in glacier geometry and ice velocity (following *Kamb and Echelmeyer* [1986]). *Truffer*'s [2004] approach substantially reduces artificial basal velocity variability generated by exactly fitting modeled surface velocity to field measurements (which contain errors), but is currently restricted to a 1-D approximation of the ice flow.

[5] A major drawback of numerical calculations of sliding using surface data is the decay of basal velocity fluctuation amplitudes with height above the bed. This leads to a corresponding amplification with depth of any errors in the measured surface velocity. Theoretical studies have applied perturbation analysis to show the amplitude decay rate for a basal velocity fluctuation under a planar slab depends on the fluctuation wavelength [*Balise and Raymond*, 1985; *Bahr et al.*, 1994; *Gudmundsson*, 2003], the nonlinearity of the ice rheology [*Bahr et al.*, 1994], and the slip ratio (defined as the ratio of basal sliding velocity to surface velocity) [*Gudmundsson*, 2003]. These studies found amplitude decay rates increase with decreasing wavelength, decreasing nonlinearity, and decreasing slip ratio. Correspondingly, error amplification with depth during inversion of surface velocity data would be low for glaciers where sliding contributes a high proportion of surface motion, and lower for nonlinearly viscous glacier ice than in a linearly viscous approximation.

[6] In this paper, the basal shear stress and sliding velocity along a 2-D long section (sometimes referred to as a "flow line") of an Alpine glacier are calculated numerically using a first-order approximation to the ice

flow equations, with nonlinear ice rheology and without the assumptions of a sliding law. Uncertainties in calculated sliding velocities are estimated by a Monte Carlo simulation, and the results are used to infer variations in subglacial conditions (bedrock roughness and water pressure) along the flow line. Error amplification rates are then compared with theoretical estimates.

2. Field Site

[7] Glacier de Tsanfleuron is located at 46°20′N, 7°15′W in the Swiss Alps and largely consists of a shallow-angled ice plateau between ~2650 and 2980 m asl, with a steeper tongue descending to the terminus at ~2500 m asl (Figure 1). Sparse debris cover over the glacier margin, and observations in ice marginal cavities and over the neighboring limestone plateau, indicate the glacier is bedrock based.

[8] Evidence for basal sliding has been found by direct measurement of basal motion (~11 mm d^{-1}) in an ice marginal cavity [*Hubbard*, 2002], and indirectly from observations of striated bedrock and regelation-related carbonate precipitates that are widespread over much of the limestone plateau exposed by recent retreat [*Hallet et al.*, 1978; *Sharp et al.*, 1989; *Hubbard and Hubbard*, 1998]. Estimated variations in water content between basal and englacial ice based on ice core observations [*Hubbard et al.*, 2000; *Tison and Hubbard*, 2000] were used to identify a rheologically soft basal ice layer [*Hubbard et al.*, 2003].

3. Methods
3.1. Surface Velocity

[9] The surface velocity field between 21 June and 19 August 2002 was determined by repeat surveying of marker stakes (Figure 2) drilled into the glacier surface, using standard surveying techniques with a Geodimeter total station [*Hubbard et al.*, 1998]. Readings were corrected for instrumental drift using a reference marker (Ref 1) fixed to bedrock adjacent to the glacier and readings from a second fixed reference (Ref 2) were used to estimate the magnitude of errors in horizontal angle. These estimates of the velocity error are required for the Monte Carlo simulation and are calculated as described below.

[10] For small errors in horizontal angle (*HA*) and vertical angle (*VA*), denoted ε_{HA} and ε_{VA} respectively, the resulting error in horizontal stake position is

$$\varepsilon_H^2 = (\varepsilon_{HA} SD \sin VA)^2 + (\varepsilon_{VA} SD \cos VA)^2 \qquad (2)$$

where *SD* is the sighted distance to the marker and ε_{HA} and ε_{VA} are in radians. *VA* was within the range 90 ± 5° for all markers, so the second term on the RHS of equation (2) is negligible (<1 mm) and is ignored. The quoted instrumental error in *SD* for the Geodimeter Total Station is 2 mm plus 1 mm per 1000 m sighted distance:

$$\varepsilon_S = 10^{-3} SD + 2. \qquad (3)$$

ε_{HA} and ε_S are assumed to be random and normally distributed and the standard deviation of Ref 2 *HA* readings is used to estimate ε_{HA} (Table 1). *HA* values closely fit a normal distribution (rms deviation 4.8%) (Figure 3) so this is not an unreasonable assumption. If *HA* increases
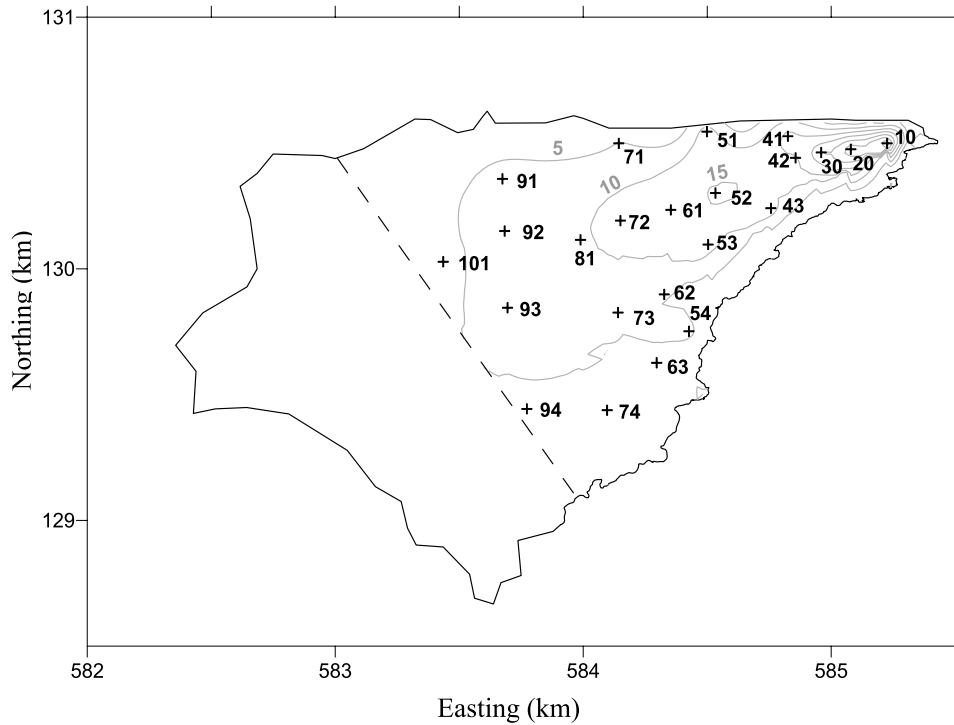
Figure 2. Easterly component of surface velocity (contours at 5 m yr^{-1} intervals) and velocity marker stake positions. Measured stake velocities were interpolated onto a grid down glacier from the dashed line. Coordinates are in Swiss Grid.

clockwise from east then errors in the easterly and northerly components of horizontal stake position are:

$$\varepsilon_{HE}^2 = (\varepsilon_{HA}SD \sin VA \sin HA)^2 + (\varepsilon_S \sin VA \cos HA)^2, \quad (4a)$$

$$\varepsilon_{HN}^2 = (\varepsilon_{HA}SD \sin VA \cos HA)^2 + (\varepsilon_S \sin VA \sin HA)^2. \quad (4b)$$

[11] The velocity data sets are not all continuous, mostly due to stake redrilling carried out in bad weather, often leaving a gap of a few days before the new stake position was surveyed. The summer velocity average is then calculated from p individual time periods which are discontinuous in time and the error for the summer velocity average is determined from a weighted sum of errors for each individual period. If there are p time intervals i of duration t_i with a total duration $T = t_1 + t_2 + \ldots + t_p$, then errors in the easterly and northerly components of mean stake velocity are:

$$\varepsilon_{VE} = \sqrt{\frac{1}{T}\sum_{i=1}^{p}\frac{2\varepsilon_{HE}^2}{t_i}}, \quad (5a)$$

$$\varepsilon_{VN} = \sqrt{\frac{1}{T}\sum_{i=1}^{p}\frac{2\varepsilon_{HN}^2}{t_i}}. \quad (5b)$$

Table 1. Estimates of Horizontal Angle Error, ε_{HA}, for Surveys at Glacier de Tsanfleuron

Survey Station	ε_{HA}, arc sec
SS1	20.1
SS2	8.0

[12] Long-section surface elevation and ice thickness (Figure 1) were measured by *Hubbard et al.* [2003] with radio echo sounding and a GPS during January 2001. Individual stake velocities, errors and ice thickness values were interpolated onto a grid using Kriging, from which the long-section profiles of velocity, velocity error, bed elevation and surface elevation were extracted. Surface velocity fields were constructed assuming a zero-velocity boundary condition at the margins.
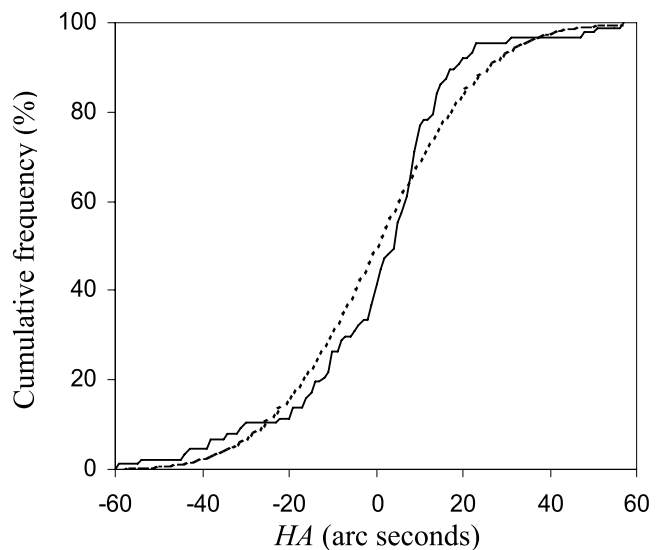

Figure 3. Cumulative frequency distribution of Ref 2 *HA* readings, summer 2002 (solid line), and the corresponding cumulative normal distribution (dashed line).

3.2. Sliding Calculated With the Shallow Ice Approximation

[13] The simplest method to calculate sliding uses the shallow ice approximation (SIA) to calculate the deformation component of the surface velocity and assumes the remaining motion is due to sliding. Longitudinal stresses are ignored and the basal shear stress τ_b is approximated by the driving stress τ_d:

$$\tau_d = -\rho g H \frac{dh}{dx} \qquad (6)$$

where H is the ice thickness, h is the surface elevation, x is the horizontal down-glacier coordinate (Figure 1), $\rho = 900$ kg m^{-3} is the ice density and $g = 9.81$ m s^{-2} is the acceleration due to gravity. Assuming A is constant with depth, the surface velocity in the SIA can easily be shown [e.g., *Van der Veen*, 1999] to be

$$u_s = \frac{2AH}{n+1}\tau_d^n + u_0 \qquad (7)$$

in which the first and second terms on the RHS are the deformation and sliding components respectively, and n is the exponent in Glen's flow law taken here to be $n = 3$. Since u_s and τ_d are known from field measurements, equation (7) can be used to provide an estimate of basal sliding.

3.3. Numerical Ice Flow Model

[14] Stress and velocity fields in the glacier were calculated using *Blatter*'s [1995] 2-D glacier flow model, described in full elsewhere [*Blatter*, 1995; *Colinge and Blatter*, 1998] and summarized briefly below. The model has previously been applied in 3-D to structural glaciology and dynamics at Haut Glacier d'Arolla [*Hubbard et al.*, 1998; *Hubbard and Hubbard*, 2000; *Nienow et al.*, 2005] and in 2-D to rheological investigations at Glacier de Tsanfleuron [*Hubbard et al.*, 2003].

[15] The glacier is bounded by the surface $h = h(x)$ and the bed $B = B(x)$ (Figure 1). u and w are the horizontal and vertical velocity components, respectively. Assumptions of incompressible ice and no basal or internal melting or freezing require

$$\frac{\partial u}{\partial x} + \frac{\partial w}{\partial z} = 0 \qquad (8)$$

[16] Steady flow is assumed, so that the force balance equations are

$$\frac{\partial \sigma_{xx}}{\partial x} + \frac{\partial \sigma_{xz}}{\partial z} = 0$$
$$\frac{\partial \sigma_{xz}}{\partial x} + \frac{\partial \sigma_{zz}}{\partial z} = \rho g \qquad (9)$$

in which σ_{ij} are components of the stress tensor. Finally the flow law $F(\tau)$ used is

$$F(\tau_{ij}) = A\left(I_{II}^2 + T_0^2\right)^{\frac{n-1}{2}}\tau_{ij} \qquad (10)$$

where A and n are the rate factor and exponent in Glen's flow law (respectively), I_{II}^2 is the second invariant of the deviatoric stress tensor τ_{ij}, and $(AT_0^{n-1})^{-1}$ is the ice viscosity in the limit $I_{II} \rightarrow 0$ [*Blatter*, 1995]. It is assumed $n = 3$. The surface boundary condition is zero shear stress parallel to the surface (i.e., $\tau_{x,s} = 0$), and the basal boundary condition is a sliding velocity that can be specified explicitly or calculated using a sliding law.

[17] Equations (8)–(10), together with the boundary conditions, provide sufficient information to calculate the stress and velocity fields in the glacier. First, equations (8) to (10) are scaled so that individual terms can be expressed as powers of the aspect ratio ε, defined as

$$\varepsilon = \frac{[H]}{[L]} \qquad (11)$$

where $[L]$ and $[H]$ are the length and thickness scales of the glacier. Since typically $[H] \ll [L]$, terms of second order in ε are discarded, and the resulting solution is a first-order approximation.

[18] The numerical solution scheme (Figure 4) splits the glacier vertically into n_z layers. u, w and τ_{xz} in each layer are calculated by integrating vertically upward from the bed to the surface using a second-order Runge-Kutta scheme, and τ_{xx} is determined algebraically. Initial values for the integration are set by the basal boundary condition, and by specifying a suitable estimate for the bed-parallel basal traction $\tau_{x,0}$. These initial values do not necessarily satisfy the surface boundary condition, and the discrepancy is used to improve the estimate of $\tau_{x,0}$:

$$\tau_{x,0}^{r+1} = \tau_{x,0}^r - \beta_\tau \tau_{x,s}^r \qquad (12)$$

where r is the iteration number, $\tau_{x,s}$ is the surface-parallel shear stress at the surface (which should be zero if the boundary condition is satisfied), and β_τ is an iteration convergence parameter. The vertical integration is then repeated with the new $\tau_{x,0}$ estimates and the procedure continues until the surface boundary condition is satisfied to within a given tolerance (specified here as 10^{-4} bar). In this numerical scheme, the first-order approximation requires the grid spacing to be greater than the local ice thickness ($\Delta x > H$). A second requirement is that the iteration procedure converges; for n_x horizontal grid points the iteration is stable provided [*Blatter*, 1995; *Müller*, 1991]:

$$0 < \beta_\tau < 2\exp(-2n_x\varepsilon) \qquad (13)$$

[19] For the long section at Glacier de Tsanfleuron (Figure 4) with a horizontal grid spacing of 100 m, $[H] = 90$ m, $[L] = 2500$ m and $n_x = 26$. Equations (11) and (13) give $0 < \beta_\tau < 0.31$ and setting $\beta_\tau = 0.1$ resulted in convergence in all model runs for $\Delta x \geq 70$ m. Below 70 m, convergence was not achieved with any values of β_τ tested from 0.001 to 0.1 and in any case the model is not valid for grid spacings shorter than the ice thickness.

[20] The model output was checked to ensure the velocity and stress fields, once normalized using *Blatter*'s [1995] scaling, were of order unity. This check provides confidence
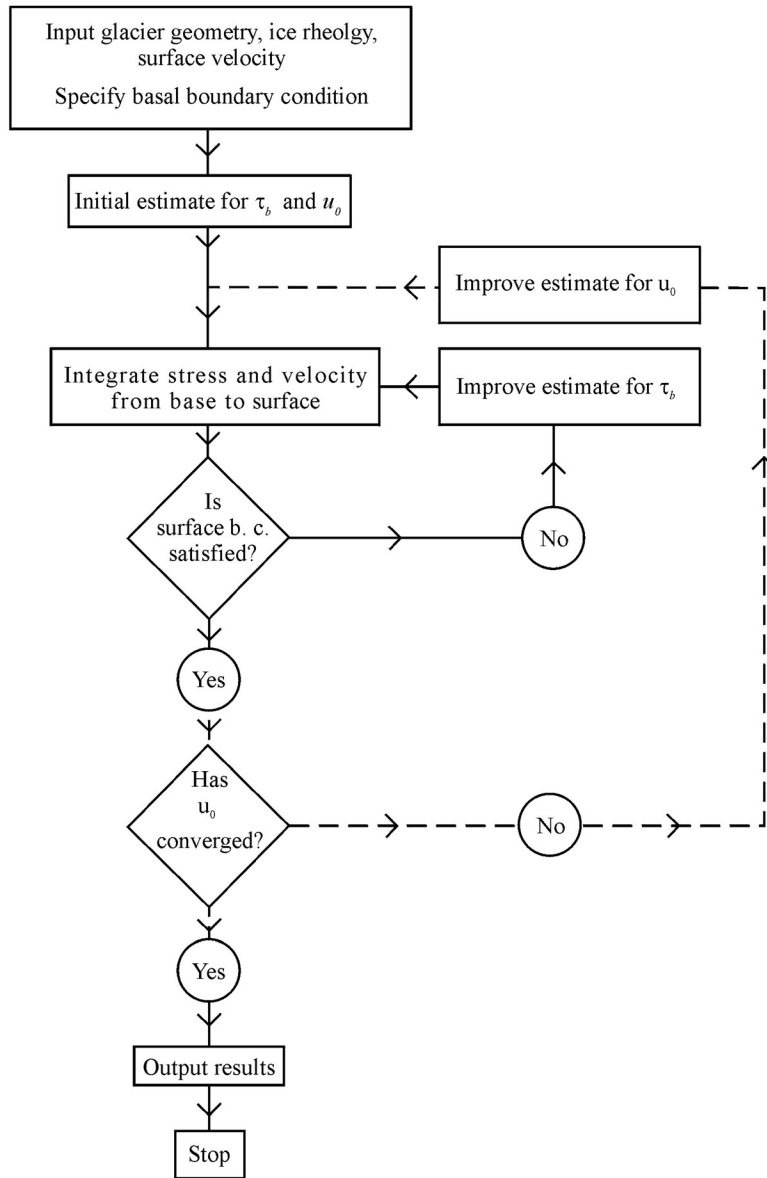
Figure 4. Block diagram of *Blatter*'s [1995] ice flow model (solid lines) and the iteration loop added in this study to calculate the basal sliding velocity (dashed lines).

that the scalings and first-order approximation used in the model are valid for the present application at Glacier de Tsanfleuron.

3.4. Monte Carlo Simulation

[21] In previous applications of this model basal sliding has been set to zero [*Hubbard et al.*, 2003], estimated using seasonal changes in surface velocity [*Hubbard et al.*, 1998], or prescribed in a mixed free slip/zero-slip basal boundary condition [*Nienow et al.*, 2005]. Here, no assumptions are made concerning sliding and instead a second iteration loop is added to the model to calculate the sliding velocity field required to match the measured and modeled surface velocity fields (Figure 4). An initial guess for the sliding velocity $u_{0,i}$ is improved in subsequent iterations by com-

paring the measured surface velocity ($u_{s,i}$) and modeled surface velocity ($u_{i,nz}$) at each grid point i:

$$u_{0,i}^{p+1} = u_{0,i}^p + \beta_v\left(u_{s,i} - u_{i,nz}^p\right) \qquad (14)$$

where p is the surface velocity iteration number, and β_v is an iteration convergence parameter. Negative velocities are set to zero. Iterations continue until the convergence criterion

$$\left|\frac{1}{4}\left(u_{i-1,nz} + 2u_{i,nz} + u_{i+1,nz}\right) - u_{s,i}\right| < \gamma \qquad (15)$$

is satisfied, where γ is a specified tolerance level for convergence taken here as 2 m yr^{-1}. A smoothed surface velocity is used in equation (15) so that small fluctuations in

Table 2. Summary of Monte Carlo Simulations 1–9[a]

Run	A, yr^{-1} bar^{-3}	n_z	Δx, m	σ_s, m yr^{-1}	$\overline{S}$, %	$\overline{E}$	Notes
1	1.2	40	100	ε_{VE}	70.9	1.64	standard parameters
2	0.6	40	100	ε_{VE}	83.8	1.64	A 50% smaller
3	1.8	40	100	ε_{VE}	57.4	1.56	A 50% larger
4	1.2	40	100	ε_{VE}	44.9	1.49	multilayer rheology
5	1.2	30	100	ε_{VE}	70.7	1.64	n_z 25% smaller
6	1.2	50	100	ε_{VE}	70.7	1.64	n_z 25% larger
7	1.2	40	200	ε_{VE}	72.3	1.38	Δx doubled
8	1.2	40	100	$\frac{1}{2}\varepsilon_{VE}$	71.6	1.15	half input errors
9	1.2	40	100	$\frac{1}{3}\varepsilon_{VE}$	71.9	1.02	third input errors

[a]Rate factor A, number of horizontal ice layers n_z, grid spacing Δx, surface velocity error σ_s, mean slip ratio $\overline{S}$, mean error amplification $\overline{E}$.

modeled surface velocity with a wavelength of $2\Delta x$ (which are numerical artifacts) do not affect convergence. Such fluctuations were substantially reduced by mixing second-order centered differences and third-order backward differences in the finite difference implementation of horizontal derivatives, but could not be removed entirely.

[22] Uncertainties in calculated sliding velocities are estimated in a Monte Carlo simulation in which the iteration routine for sliding is completed 10000 times, each time with a surface velocity field that is slightly perturbed from its measured configuration. Perturbations are random and normally distributed, with the standard deviation (σ_s) determined by the error associated with the measured surface velocities (equation (5)) so that $\sigma_s = \varepsilon_{VE}$.

[23] Random numbers uniformly distributed in the range (0,1) were generated with a function described by *Press et al.* [1993]. Numbers generated by this function are free from sequential correlation (unlike, for example, the more easily implemented 'rand' intrinsic function in FORTRAN) and have an estimated period of $\sim 2 \times 10^{18}$. The seed (initial value) for the generator was based on the date and time at the start of the simulation and is therefore unique for each run. To convert the uniform distribution to a normal distribution, each random number was treated as the probability of obtaining a value less than δ in a normal distribution with mean 0 and standard deviation 1. If the error associated with the velocity at point i is assumed to be normally distributed with standard deviation $\sigma_{s,i}$, the perturbed surface velocity U_i is

$$U_i = u_{s,i} + \sigma_{s,i}\delta_i. \tag{16}$$

Surface velocities U_i are the input to the iteration scheme for sliding velocity described above. In the iteration loop (equation (14)) initial values for $u_{0,i}$ are random and are uniformly distributed in the range $(0, 2u_{s,i})$. If the convergence criterion (equation (14)) is satisfied within p_{max} iterations, the solution for u_0 is accepted. If not, the solution is ignored and a new set of U_i is generated. Where convergence does occur, experiment shows all initial values tested converge to the same result. Decreasing γ improves the match but convergence is less likely.

[24] The Monte Carlo simulation was initially run with nine configurations of model parameters (Table 2) to investigate (1) the effects of ice rheology (runs 1–4), (2) vertical grid spacing (runs 1, 5, and 6), (3) horizontal grid spacing (runs 1 and 7), and (4) the magnitude of errors

in input surface velocity (runs 1, 8, and 9) on calculated sliding velocities. To compare results from each run, the long-section averaged contribution of sliding to surface motion ($\overline{S}$) and the long-section averaged error amplification ($\overline{E}$) for grid points $i = 1, 2, \ldots, n_x$ are defined as

$$\overline{S} = \frac{1}{n_x}\sum_i \frac{u_{0,i}}{u_{s,i}} \tag{17}$$

$$\overline{E} = \frac{1}{n_x}\sum_i \frac{\sigma_{0,i}}{\sigma_{s,i}}. \tag{18}$$

S is equivalent to the slip ratio [*Gudmundsson*, 2003] and E is a measure of how errors in surface velocity are amplified at the bed. $E < 1$ if the uncertainty in calculated sliding is less than the error in surface velocity (when errors are damped) and $E > 1$ if errors are amplified with depth. Values of E obtained in the Monte Carlo simulation can be compared with the expected error amplification predicted from theoretical work [*Bahr et al.*, 1994]. From equations 16, 22 and 25 of *Bahr et al.* [1994] the downward amplification of a small surface perturbation ΔX_s in quantity X (where X can be a stress or velocity component) leads to a perturbation ΔX_0 at the bed with an amplitude given approximately by

$$\frac{\Delta X_0}{\Delta X_s} = \exp\left(1.155\pi \frac{H}{\lambda}\right) \tag{19}$$

where λ is the perturbation wavelength. Treating the perturbations ΔX as uncertainties in surface and basal velocities, so that $\Delta u_s = \sigma_s$ and $\Delta u_0 = \sigma_0$, then we expect

$$E = \frac{\sigma_0}{\sigma_s} = \exp\left(1.155\pi \frac{H}{\lambda}\right). \tag{20}$$

[25] From equation (20) it can be seen E increases as λ decreases so that short wavelength perturbations dominate the downward propagation of errors. In the numerical model applied here the shortest perturbation wavelength possible is two grid spacings ($2\Delta x$) for which E can be estimated by setting $\lambda = 2\Delta x$. With $H = 90$ m (a typical value on the plateau at Tsanfleuron) and $\Delta x = 100$ m, equation 20 gives an approximate value of $E = 5.1$ indicating uncertainties in calculated sliding velocities should be 5 times greater than the error in surface velocity.
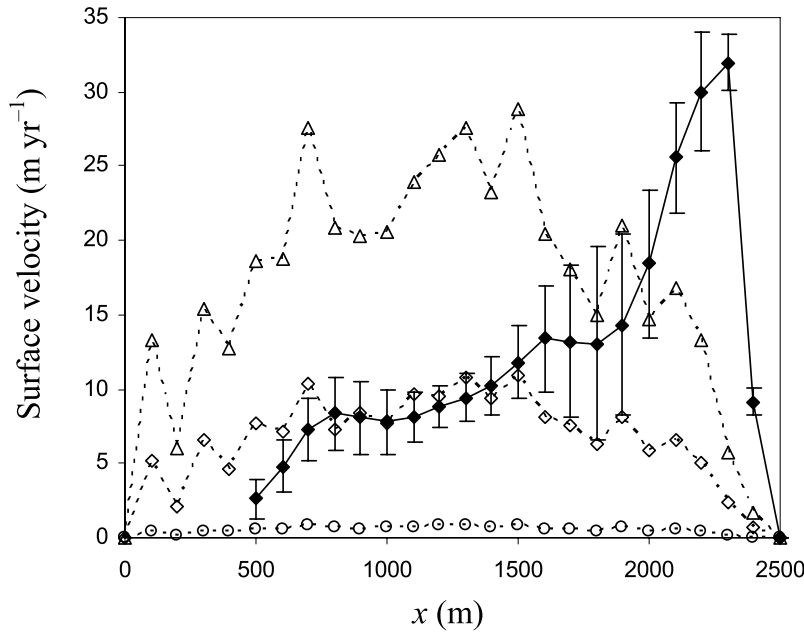
Figure 5. Long-section surface velocity: field data (solid line with error bars) and modeled surface velocities (dashed lines) with no sliding using $A = 0.21$ yr^{-1} bar^{-3} (circles), $A = 7.0$ yr^{-1} bar^{-3} (triangles), and the multilayer ice rheology (see text and Table 4) with $A_{UZ} = 1.2$ yr^{-1} bar^{-3} (diamonds).

For H = 35 m (a typical value in the tongue), error amplification is reduced to $E = 1.9$. Other theoretical estimates of vertical amplitude transfer [e.g., *Balise and Raymond*, 1985; *Gudmundsson*, 2003] are less suitable for comparison with the ice flow model used here because they do not use a nonlinear ice rheology.

3.5. Application of a Sliding Law

[26] Results generated in the Monte Carlo simulation can be used to infer variations in bed roughness and subglacial water pressure by assuming a sliding law of the form of equation (1). Assuming $b = 1$, equation (1) can be rewritten as

$$\frac{k}{N} = \frac{u_0}{\tau_b^a} \tag{21}$$

in which τ_b and u_0 are calculated in the model. The variation in the sliding law parameter K defined as $K = k/N$ can then be calculated along the long section.

4. Results

4.1. Surface Velocity

[27] Velocity measurements for 23 stakes from 21 June to 19 August 2002 show mean velocity magnitudes ranging from 3.7 to 46.4 m yr^{-1} (Table 3) with a general down-glacier increase in velocity toward the tongue (Figure 5) and flow directions typically within 10° of east.

[28] To estimate whether ice deformation alone can account for the observed surface velocity field, the ice flow model was run with zero sliding for three rate factors: (1) $A = 0.21$ yr^{-1} bar^{-3} (*Paterson*'s [1994] recommended rate factor for temperate ice), (2) $A = 7.0$ yr^{-1} bar^{-3} (optimized rate factor for Glacier de Tsanfleuron with constant A

[*Hubbard et al.*, 2003]), and (3) depth-dependent A (Table 4) with values depending on the estimated vertical variation in water content in ice cores extracted from Glacier de Tsanfleuron in 1996 and 1997 [*Hubbard et al.*, 2003]. None of these rheologies can reproduce the observed pattern in surface velocity (Figure 5), in particular the sharp velocity increase measured in the tongue at $x > 1800$ m. The *Hubbard et al.* [2003] single-layer value for A (7 yr^{-1} bar^{-3}) is too large, since surface velocities are mostly overestimated while *Paterson*'s [1994] recommended value is likely to be too small, unless sliding contributes almost all of the total ice motion. Velocities calculated with the multilayer ice rheology are consistent with measurements over much of the glacier (within errors) but again severely underestimate velocities in the tongue.

4.2. Basal Sliding Velocity and Shear Traction

[29] Over the parameter ranges tested (Table 2), the flow line-averaged slip ratio calculated by the first-order model ($\overline{S}$) is almost independent of the grid resolution (Δx and n_z) and error in measured surface velocity (σ_s) (Table 2). The calculated pattern of sliding (Figure 6) also shows little change with varying n_z, and doubling Δx from 100 m to 200 m has little effect on u_0 for $x < 1800$ m (Figure 7) but results in small (<5 m yr^{-1}) variations in the tongue at 2000 m and 2200 m. Calculated sliding velocities are strongly dependent on A (Figure 7a and Table 2) and, as expected, $\overline{S}$ decreases as A increases since an increasing proportion of ice motion occurs via internal deformation. Adding a soft basal ice layer (run 4) reduces $\overline{S}$ from 71% to 45% but does not change the overall pattern of sliding and in all cases u_0 generally increases down glacier to ~30 m yr^{-1} (Figures 6a and 7) so that sliding accounts for at least 80% of the total ice motion in the final ~500 m of the glacier.

Table 3. Stake Velocities Measured at Glacier de Tsanfleuron[a]

Stake	T, days	v, m yr^{-1}	θ, deg	v_E, m yr^{-1}	v_N, m yr^{-1}	ε_{VE}, m yr^{-1}	ε_{VN}, m yr^{-1}
10	7.3	46.4	63	40.7	−20.8	0.7	1.2
20	7.3	33.9	98	34.1	−4.7	0.6	1.5
30	4.5	25.2	103	24.3	−5.5	2.6	6.2
41	28.6	17.5	85	17.2	1.5	1.6	4.7
42	27.0	14.2	85	14.4	0.7	2.2	5.1
43	19.6	12.4	92	12.3	−0.4	5.5	5.8
51	24.8	12.4	95	12.4	−1.1	1.1	2.6
52	13.1	15.7	98	15.6	−2.2	6.2	5.1
53	26.3	11.7	92	11.7	−0.4	2.2	0.7
54	19.1	7.7	64	6.9	3.2	4.7	0.4
61	43.0	13.9	85	13.7	1.5	2.2	0.6
62	12.0	5.8	75	5.6	1.4	8.0	0.3
63	22.0	3.7	107	3.4	−1.0	4.4	0.4
71	17.1	–	–	5.5	–	0.7	–
72	28.1	–	–	12.0	–	1.8	–
73	38.8	–	–	5.2	–	2.2	–
74	29.0	–	–	2.8	–	2.2	–
81	33.9	9.4	93	9.4	−0.7	0.7	0.4
91	28.3	8.0	104	8.0	−1.8	1.1	5.1
92	28.1	9.5	83	9.5	1.2	2.6	4.6
94	29.1	8.4	111	7.9	−2.9	1.0	1.2
95	43.8	4.0	91	4.0	−0.1	1.1	0.7
101	25.6	7.3	29	2.6	6.9	1.8	3.3

[a]Time series length T; stake speed v and direction θ defined with $\theta = 0°$ in northerly direction and increasing clockwise; easterly and northerly stake velocity components v_E and v_N and their associated errors ε_{VE} and ε_{VN}. Only the easterly velocity component of row 7 stakes (71 to 74) is available, as these were placed due south of the survey station and were not fitted with marker prisms.

[30] The calculated pattern of basal shear traction τ_b in the first-order model can be compared with the SIA, in which τ_b is approximated by the driving stress τ_d (equation (6)). With $A = 1.2$ yr^{-1} bar^{-3}, the basal traction calculated by both methods (Figure 6b) is similar: typically $|\tau_d - \tau_b| < 0.1$ bar away from the end points. Taking $\overline{\tau_{xx}}$ to be the depth-averaged longitudinal stress at each horizontal grid point in the first-order model, the long-section averaged value of $|\overline{\tau_{xx}}/\tau_d| = 0.37$ shows the magnitude of the longitudinal stress is approximately a third of the driving stress.

4.3. Error Amplification

[31] In run 1, velocity error amplification occurs with depth and, averaged along the flow line, uncertainties in basal sliding are 64% greater than the estimated surface velocity errors (i.e., $\overline{E} = 1.64$). Amplification occurs for all grid points except $x = 500$ m (Figure 8) and leads to wide 90% confidence intervals on calculated sliding velocities (Figure 6a). The input error (σ_s) itself also affects error amplification and when σ_s is reduced, $\overline{E}$ is correspondingly reduced (Table 2). However, the general down-glacier pattern of E (i.e., the position of maxima and minima) remains similar for all model runs and is typified by runs 1 and 8 (Figure 8). $\overline{E}$ is independent of n_z over the range tested and shows only a slight change with A (Table 2).

[32] Doubling the horizontal grid spacing Δx from 100 m to 200 m reduces $\overline{E}$ from 1.64 to 1.38. To investigate this further, sliding was calculated in a second set of Monte Carlo simulations with $\Delta x = 70, 80, \ldots, 240$ m where the lower bound on Δx is set by the convergence limit of the iteration loop for τ_b and the upper bound is set to ensure at least 10 grid points. Results show $\overline{E}$ decreases with increasing Δx (Figure 9) while variations in $\overline{S}$ remain small (standard deviation 2.5%). The best fit curve for $\overline{E}$ is

$$\overline{E} = 3.7\Delta x^{-0.18} \qquad (22)$$

with $R^2 = 0.94$ (Figure 9). Calculated values of error amplification are generally less than the theoretical estimates for glaciers between 35 and 90 m thick (Figure 10), and also the functional form of equation (20) is not suitable to describe the relationship between $\overline{E}$ and Δx found in the Monte Carlo simulation.

4.4. Application of a Sliding Law

[33] The down-glacier variation in K (Figure 11) was calculated for $a = 2$ and $a = 3$ in equation (21) using modeled values of u_0 and τ_b. Median values of K are found to be highly variable along the long section, and the distance between the 5th and 95th percentiles indicates uncertainties in K are large: often over an order of magnitude. However, the peaks at $x = 900$ m and $x = 2200$ m lie outside these uncertainties and are common to both values of a. The first of these peaks corresponds to a minimum in τ_b (Figure 6b) and a bedrock depression (Figure 1) while there are no obvious features in the bed profile corresponding to the peak at $x = 2200$ m.

5. Summary and Discussion

[34] With zero sliding, ice deformation alone cannot account for the high velocities in the tongue with any of the rate factor distributions tested (Figure 5), indicating that either (1) sliding forms an important contribution to the total ice motion over at least part of the glacier or that (2) ice in

Table 4. Vertical Variation in Rate Factor of *Hubbard et al.*'s [2003] Multilayer Ice Rheology Model[a]

Layer	Depth	Rate factor
Upper zone	$0.175H < z < H$	A_{UZ}
Lower zone	$0.025H < z < 0.175H$	$1.8A_{UZ}$
Basal zone	$0 < z < 0.025H$	$10.7A_{UZ}$

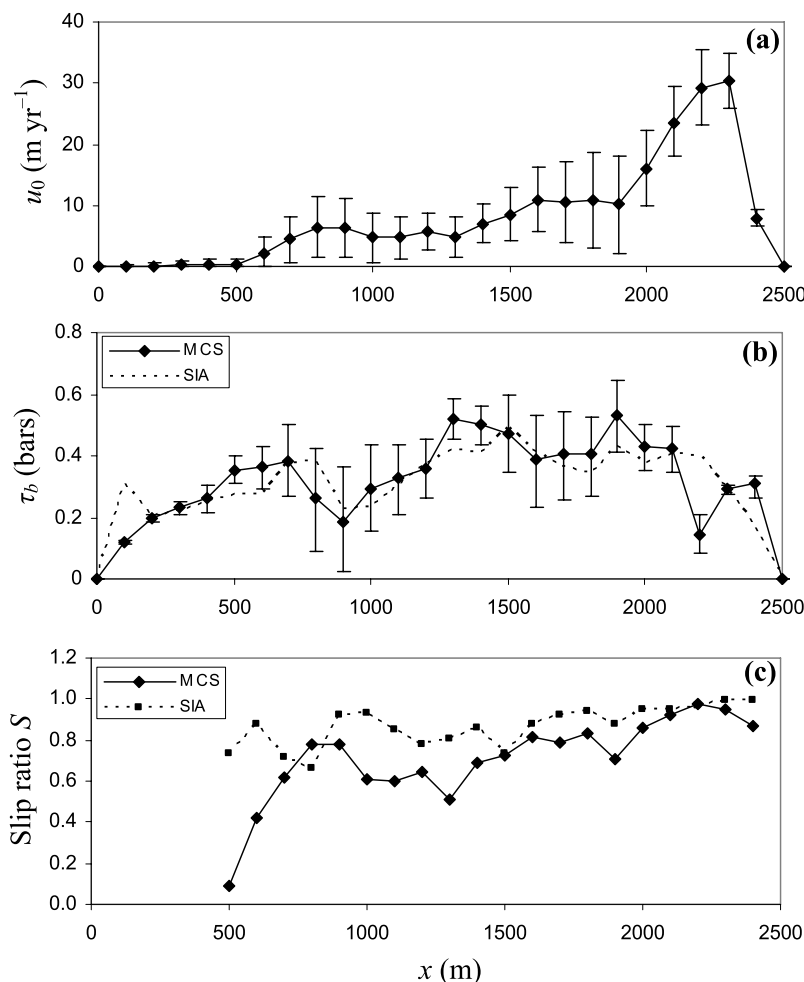[a]The vertically averaged rate factor is $1.36A_{UZ}$.

Figure 6. Monte Carlo simulation results for run 1 (see Table 2). (a) Mean basal sliding velocity u_0 with 90% confidence intervals (error bars mark 5th and 95th percentiles of 10,000 solutions). (b) Same as Figure 6a but for basal shear traction τ_b. The dashed line is the basal shear stress calculated in the SIA. (c) Variation in slip ratio S for the SIA (dashed line) and Monte Carlo simulation (solid line).

the tongue is relatively soft in comparison with ice on the plateau. Since a very large increase in A in the tongue would be required to account for the observed velocity field, the contribution of sliding is the more likely of the above two possibilities. The SIA and first-order ice flow model were both used to calculate the basal sliding distribution necessary to account for the observed velocity field and both show a down-glacier increase in sliding. Accelerating flow, and a corresponding extensive stress regime in the majority of the glacier, results in extensive longitudinal stresses that are not accounted for in the SIA and leads to the lower estimate of internal deformation (i.e., higher slip ratio) apparent from comparison of results obtained using both methods (Figure 6c).

[35] Insensitivity of the predicted distribution of sliding to the grid spacing parameters (Δx and n_z) provides confidence that calculated sliding velocities are not artifacts of the model algorithm or configuration.

5.1. Rate Factor A

[36] Calculated sliding velocities decrease as A increases, due to the increasing contribution of internal deformation to ice flow. However, while the surface velocity is the same in each model run, the horizontal ice transport (given by the vertically integrated ice velocity) is greater for those runs with greater sliding. Currently, the choice of A is poorly constrained. Values of A used by *Hubbard et al.* [2003] for this long section are likely to be too large since their optimization method assumed zero sliding. *Paterson*'s [1994] recommended value of $A = 0.12$ bar^{-3} yr^{-1} clearly gives modeled surface velocities that are too small (Figure 5), reaching only 5 to 10% of the measured surface velocity. This result is in contrast to other recent studies where A has been optimized and found to be a factor of 2 to 3 less than Paterson's value [e.g., *Hubbard et al.*, 1998; *Gudmundsson*, 1999; *Truffer et al.*, 2001]. In the present model the high value of A may be due to the absence of transverse stresses which could soften the ice by increasing the magnitude of the stress invariant I_{II} (equation (10)), or in the multilayered rheology may reflect underestimates of the basal ice thickness or basal ice enhancement factors.

[37] Assuming the model with zero sliding underestimates the surface velocity, the upper bound $A < 2.1$ yr^{-1} bar^{-3} is
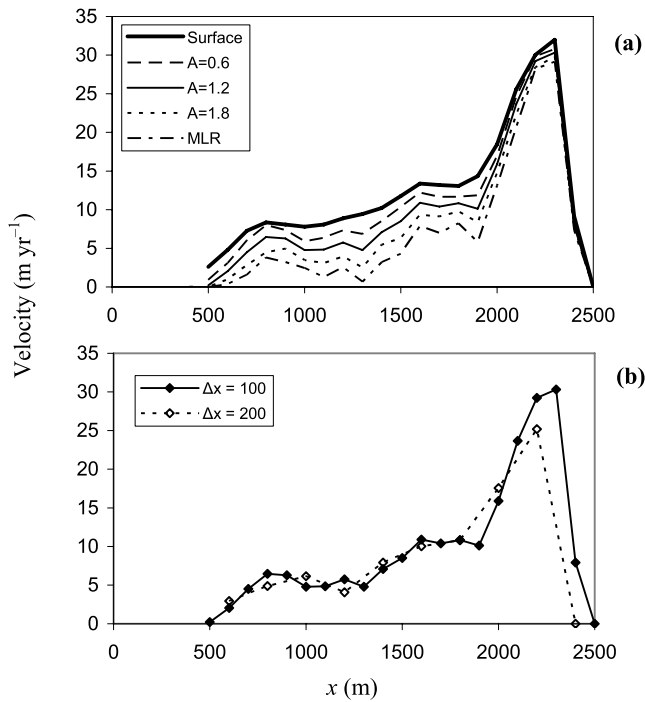
Figure 7. (a) Measured surface velocity and calculated patterns of basal sliding obtained with A = 0.6, 1.2, and 1.8 yr^{-1} bar^{-3} and for the multilayer rheology with A_{UZ} = 1.2 yr^{-1} bar^{-3}; (b) sliding velocity calculated with Δx = 100 and 200 m.
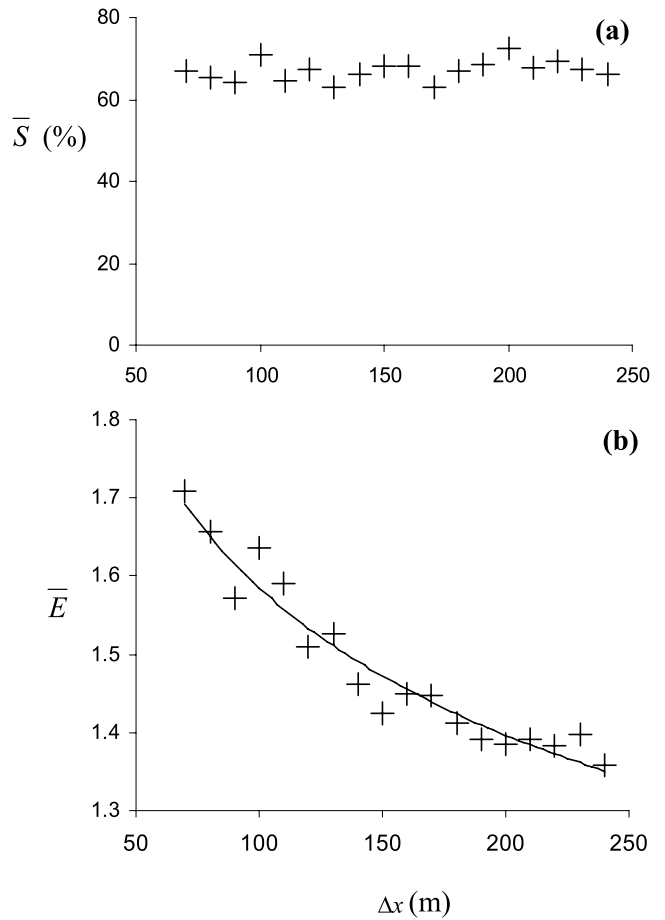

Figure 9. (a) Slip ratio $\overline{S}$ and (b) mean error amplification $\overline{E}$ for varying grid spacing Δx. The regression curve in Figure 9b is $\overline{E}$ = 3.7$\Delta x^{-0.18}$ (R^2 = 0.94).

necessary to ensure that the modeled velocity is lower than the measured velocity (within the estimated errors) over the entire long section; higher values of A lead to an overestimate of the surface velocity in the central third of the glacier
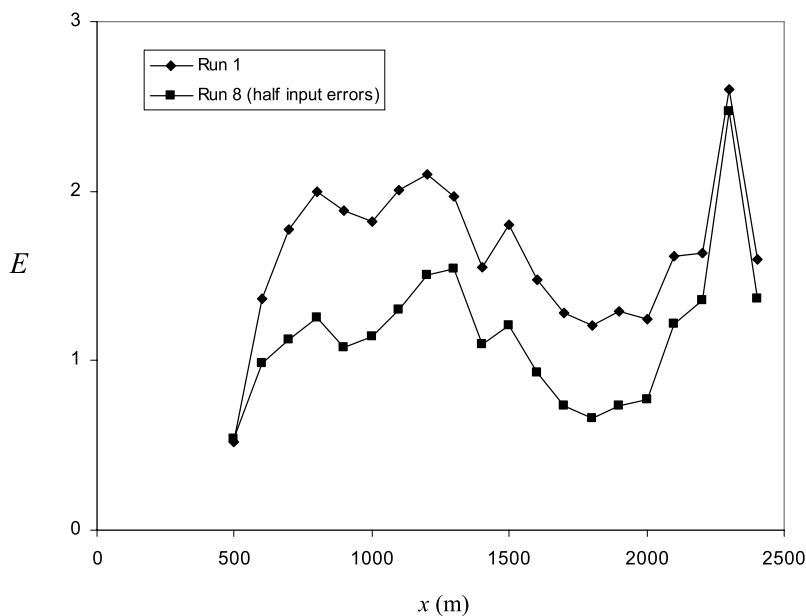

Figure 8. Flow line variability in error amplification $E = \sigma_0/\sigma_s$ for run 1 (standard parameters) and run 8 (half input errors).
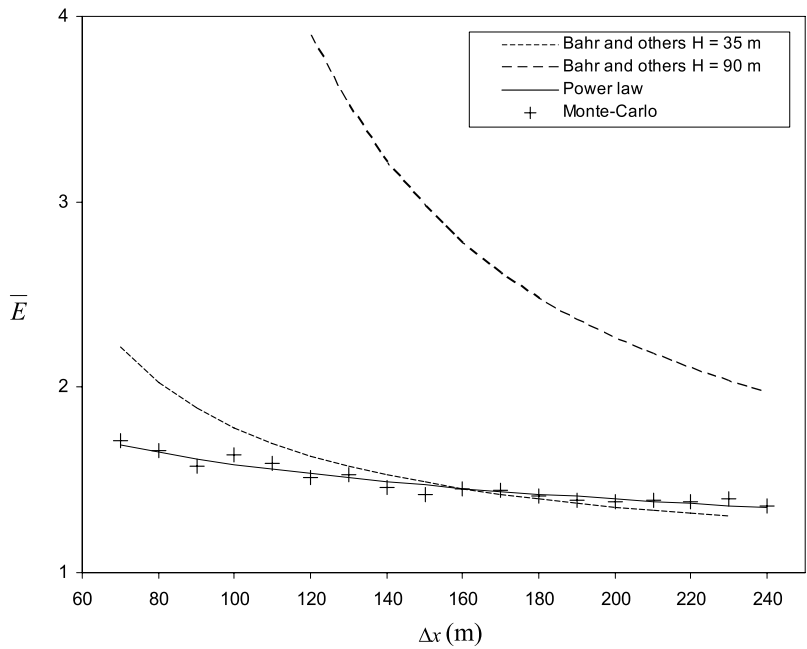
Figure 10. Comparison of error amplification $\overline{E}$ calculated in the Monte Carlo simulation (crosses) and in a theoretical study [*Bahr et al.*, 1994] with ice thicknesses $H = 35$ m (short-dashed line) and $H = 90$ m (long-dashed line). The best fit power law regression curve for the Monte Carlo results is also shown (solid line).

that cannot be countered by reducing sliding. A more tightly constrained estimate for A is not possible without further field data, such as ice temperature or in situ deformation measurements from borehole repeat inclinometry or tilt cells.

[38] In addition to the rate factor A, the second parameter in the ice rheology (equation (10)) is the exponent n. While almost all existing ice flow models take $n = 3$ there is evidence to suggest the dominant ice deformation process
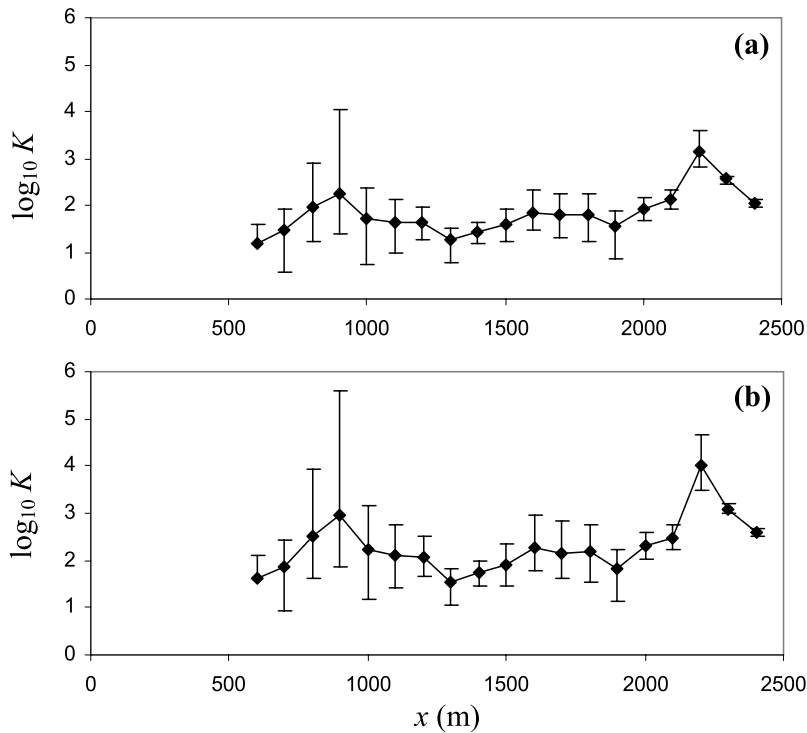

Figure 11. Calculated values of K from equation (16) with (a) $a = 2$ and (b) $a = 3$. Error bars and points mark the 5th, 50th (median), and 95th percentiles. The lower error bar is missing for $x = 600$ m as the 5th percentile is $K = 0$ in both cases.

may vary with stress and that $n < 3$ may be more appropriate for thin ice: e.g., $n = 1$ best explained borehole deformation measurements in the upper 115 m of Worthington Glacier (Alaska) [*Marshall et al.*, 2002] and $n = 1.8$ has been found in laboratory studies at low stresses [*De La Chapelle et al.*, 1999; *Goldsby and Kohlstedt*, 2001]. The incorporation of these alternative flow law exponents therefore warrants further work, in particular for thin glaciers such as Glacier de Tsanfleuron. Since A and n can be varied freely for each grid point in the *Blatter* [1995] model applied here, the possibility of using a variable ice rheology in the Monte Carlo simulation is a clear advantage of this inversion algorithm over equivalent 1-D methods [e.g., *Truffer*, 2004].

5.2. Coefficient k in the Sliding Law

[39] All model runs indicate that higher surface velocities in the glacier tongue are due to relatively rapid sliding up to at least 80% of the surface velocity (Figure 7). There is good evidence from dye tracing studies of the subglacial hydrology [*Grust*, 2004] and observations of meltwater drainage emerging along the southeastern margin that most meltwater reaching the bed drains rapidly into the limestone bedrock, so high water pressure (low N) in the tongue is unlikely. Therefore the higher sliding rates in this region, which coincide with a peak in K at $x = 2200$ m (Figure 11) are most likely due to an increase in k rather than decrease in N. This could be due to relatively steep bedrock with few reverse slopes (low roughness), combined with extensive cavities under the relatively thin ice. Extensive cavity formation is consistent with studies of basal ice in this area which point to its formation in and around basal cavities [*Tison and Lorrain*, 1987]. At the up-glacier peak in K ($x = 900$ m) thicker ice and lower sliding rates suggest a minimum in N is more likely, since the bedrock depression at $x = 900$ m may trap water. However, the possibility of an increase in k, or a combination of both these effects, cannot be discounted.

[40] Variations in K calculated with this method should be treated with caution since (1) there is little field evidence to support a sliding law of the type used here (or of any other type) and (2) the error bars on K are very large. Also, at many glaciers where the surface and sliding velocities are diurnally or seasonally variable, the interpretation of a single sliding distribution obtained from the seasonally averaged surface velocity is problematic since it is unclear exactly what the calculated distribution represents. At Tsanfleuron this averaging is unlikely to be a problem, since over the upper portion of the stake network there was no change (within the errors) in surface velocity between summer 2002 and spring 2003 [*Chandler*, 2005]. Also, the discharge stream leaving the snout is very small in comparison with similarly sized glaciers in this area suggesting a large portion of meltwater reaching the bed drains into the underlying permeable limestone bedrock, preventing the increases in subglacial water pressure necessary to generate increases in sliding during the spring or summer.

5.3. Error Amplification

[41] Uncertainty in the results increases with decreasing Δx (Figure 9), broadly consistent with previous work on transfer functions in which dampening of basal perturbations is greater for shorter perturbation wavelengths (above). Applying this theory to the present study, using a smaller Δx leads to incorporation of shorter wavelength variations in the calculated sliding velocity field, for which error amplification is greater.

[42] Regression analysis (equation (22)) suggests the functional relationship between $\overline{E}$ and Δx may be best described by a power law, rather than the form of equation (20) derived by *Bahr et al.* [1994]. Also, $\overline{E}$ is smaller than their study would suggest (Figure 10). Two major restrictions apply to the derivation of equation (20): first that the surface velocity perturbations are small (applied to the present study, this requires $\sigma_s \ll u_s$), and second that the flow is strongly compressive or strongly extensive (i.e., $\tau_{xx} \gg \tau_{xy}$). The first of these restrictions is not satisfied at Tsanfleuron since the input surface velocity errors are quite large (up to 30% of u_s). Therefore it might be expected for $\overline{E}$ to increase toward the *Bahr et al.* [1994] estimate as σ_s becomes small. However, this is not the case since $\overline{E}$ decreases with decreasing σ_s (Table 2). The second restriction is also invalid at Tsanfleuron since the magnitude of longitudinal stresses is typically a third of the driving stress. Assuming this is the principal reason for the discrepancy between the empirical and theoretical estimates of $\overline{E}$, a numerical solution to the theory of *Bahr et al.* [1994] would be warranted to remove the restrictions required in the analytic solution. In addition, application of the present algorithm to longer glaciers would allow a more detailed analysis of the relationship between $\overline{E}$ and Δx since a wider range of Δx could be investigated.

6. Conclusions

[43] The Monte Carlo simulation has proved to be a useful method of determining the sliding velocity and basal shear stress fields, with error bounds, from a known ice mass geometry and surface velocity. The algorithm can be easily applied to any ice mass, in either two or three dimensions, provided the convergence criteria are met and that the ice rheology is adequately constrained. Uncertainties in calculated sliding velocities are a power law function of the horizontal grid spacing and are higher than the errors in surface velocity, but are smaller than previous theoretical estimates suggest and can be reduced to an acceptable level by an appropriate choice of horizontal grid spacing.

References

Bahr, D. B., T. W. Pfeffer, and M. F. Meier (1994), Theoretical limitations to englacial velocity calculations, *J. Glaciol.*, *40*, 509–517.

Balise, M. J., and C. F. Raymond (1985), Transfer of basal sliding variations to the surface of a linearly viscous glacier, *J. Glaciol.*, *31*, 308–318.

Bindschadler, R. (1983), The importance of pressurized subglacial water in separation and sliding at the glacier bed, *J. Glaciol.*, *29*, 3–19.

Bindschadler, R. A., W. D. Harrison, C. F. Raymond, and R. Crosson (1977), Geometry and dynamics of a surge-type glacier, *J. Glaciol.*, *18*, 181–194.

Blake, E. W., U. H. Fischer, and G. K. C. Clarke (1994), Direct measurement of sliding at the glacier bed, *J. Glaciol.*, *40*, 595–599.

Blatter, H. (1995), Velocity and stress fields in grounded glaciers: A simple algorithm for including deviatoric stress gradients, *J. Glaciol.*, *41*, 333–344.

Chandler, D. M. (2005), Measuring and modelling glacier sliding, Ph.D. thesis, Univ. of Wales, Aberystwyth, U. K.

Cohen, D., R. L. Hooke, N. R. Iverson, and J. Kohler (2000), Sliding of ice past an obstacle at Engabreen, Norway, *J. Glaciol.*, *46*, 599–610.

Colinge, J., and H. Blatter (1998), Stress and velocity fields in glaciers: Part I. Finite-difference schemes for higher-order glacier models, *J. Glaciol.*, *44*, 448–466.

De la Chapelle, S., H. Milsch, O. Castelnau, and P. Duval (1999), Compressive creep of ice containing a liquid intergranular phase: Rate-controlling processes in the dislocation creep regime, *Geophys. Res. Lett.*, *26*(2), 251–254.

Fastook, J. L., H. H. Brecher, and T. J. Hughes (1995), Derived bedrock elevations, strain rates and stresses from measured surface elevations and velocities: Jakobshavns Isbrae, Greenland, *J. Glaciol.*, *41*, 161–173.

Gerrard, J. A. F., M. F. Perutz, and A. Roch (1952), Measurement of the velocity distribution along a vertical line through a glacier, *Proc. R. Soc. London, Ser. A*, *213*(1115), 546–558.

Goldsby, D. L., and D. L. Kohlstedt (2001), Superplastic deformation of ice: Experimental observations, *J. Geophys. Res.*, *106*(B6), 11,017–11,030.

Grust, K. (2004), The hydrology and dynamics of a glacier on limestone, Ph.D. thesis, Univ. of Glasgow, Glasgow, U. K.

Gudmundsson, G. H. (1999), A three-dimensional numerical model of the confluence area of Unteraargletscher, Bernese Alps, Switzerland, *J. Glaciol.*, *45*, 219–230.

Gudmundsson, G. H. (2003), Transmission of basal variability to a glacier surface, *J. Geophys. Res.*, *108*(B5), 2253, doi:10.1029/2002JB002107.

Gudmundsson, G. H., A. Bauder, M. Luthi, U. H. Fischer, and M. Funk (1999), Estimating rates of basal motion and internal ice deformation from continuous tilt measurements, *Ann. Glaciol.*, *28*, 247–252.

Haefeli, R. (1951), Some observations on glacier flow, *J. Glaciol.*, *1*, 496–501.

Hallet, B., R. D. Lorrain, and R. Souchez (1978), The composition of basal ice from a glacier sliding over limestones, *Bull. Geol. Soc. Am.*, *89*, 314–320.

Hanson, B. (1995), A fully 3–dimensional finite-element model applied to velocities on Storglaciaren, Sweden, *J. Glaciol.*, *41*, 91–102.

Harbor, J. M. (1992), Application of a general sliding law to simulating flow in a glacier cross section, *J. Glaciol.*, *38*, 182–190.

Harbor, J., M. Sharp, L. Copland, B. Hubbard, P. Nienow, and D. Mair (1997), Influence of subglacial drainage conditions on the velocity distribution within a glacier cross section, *Geology*, *25*(8), 739–742.

Harper, J. T., H. F. Humphrey, and W. T. Pfeffer (1998), Three-dimensional deformation measured in an Alaskan glacier, *Science*, *281*(5381), 1340–1342.

Harrison, W. D., and B. Kamb (1970), Direct measurement of sliding velocity at the base of a glacier, *Eos Trans. AGU*, *51*, 431.

Hodge, S. M. (1974), Variations in the sliding of a temperate glacier, *J. Glaciol.*, *13*(69), 349–369.

Hooke, R. L., P. Holmlund, and N. R. Iverson (1987), Extrusion flow demonstrated by bore-hole deformation measurements over a Riegel, Storglaciaren, Sweden, *J. Glaciol.*, *33*, 72–78.

Hooke, R. L., V. A. Pohjola, P. Jansson, and J. Kohler (1992), Intraseasonal changes in deformation profiles revealed by borehole studies, Storglaciaren, Sweden, *J. Glaciol.*, *38*, 348–358.

Hubbard, A. (2000), The verification and significance of three approaches to longitudinal stresses in high-resolution models of glacier flow, *Geogr. Ann., Ser. A*, *82*(4), 471–487.

Hubbard, A., and B. Hubbard (2000), The potential contribution of high-resolution glacier flow modelling to structural glaciology, in *Deformation of Glacial Materials*, edited by A. J. Maltman, B. Hubbard, and M. J. Hambrey, *Geol. Soc. Spec. Publ.*, *176*, 135–146.

Hubbard, A., H. Blatter, P. Nienow, D. Mair, and B. Hubbard (1998), Comparison of a three-dimensional model for glacier flow with field data from Haut Glacier d'Arolla, Switzerland, *J. Glaciol.*, *44*, 368–378.

Hubbard, B. (2002), Direct measurement of basal motion at a hard-bedded temperate glacier: Glacier de Tsanfleuron, Switzerland, *J. Glaciol.*, *48*, 1–8.

Hubbard, B., and A. Hubbard (1998), Bedrock surface roughness and the distribution of subglacially precipitated carbonate deposits: Implications for formation at Glacier de Tsanfleuron, Switzerland, *Earth Surf. Processes Landforms*, *23*(3), 261–270.

Hubbard, B., J. L. Tison, L. Janssens, and B. Spiro (2000), Ice-core evidence of the thickness and character of clear-facies basal ice: Glacier de Tsanfleuron, Switzerland, *J. Glaciol.*, *46*, 140–150.

Hubbard, B., A. Hubbard, H. M. Mader, J. L. Tison, K. Grust, and P. Nienow (2003), Spatial variability in the water content and rheology of temperate glaciers: Glacier de Tsanfleuron, Switzerland, *Ann. Glaciol.*, *37*, 1–6.

Kamb, B., and K. A. Echelmeyer (1986), Stress-gradient coupling in glacier flow: I. Longitudinal averaging of the influence of ice thickness and surface slope, *J. Glaciol.*, *32*(111), 267–284.

Le Meur, E., and C. Vincent (2003), A two-dimensional shallow ice-flow model of Glacier de Saint-Sorlin, France, *J. Glaciol.*, *49*(167), 527–538.

Lliboutry, L. (1995), Correspondance: Why calculated basal drags of ice streams can be fallacious, *J. Glaciol.*, *41*(137), 204.

Marshall, H. P., J. T. Harper, W. T. Pfeffer, and N. F. Humphrey (2002), Depth-varying constitutive properties observed in an isothermal glacier, *Geophys. Res. Lett.*, *29*(23), 2146, doi:10.1029/2002GL015412.

Müller, H. C. (1991), Une méthode iterative simple pour résoudre les équations de mouvement d'un glacier, mémoire de diplôme en mathématique, Univ. de Genève, Geneva, Switzerland.

Nienow, P. W., A. L. Hubbard, B. P. Hubbard, D. M. Chandler, D. W. F. Mair, M. J. Sharp, and I. C. Willis (2005), Hydrological controls on diurnal ice flow variability in valley glaciers, *J. Geophys. Res.*, *110*, F04002, doi:10.1029/2003JF000112.

Paterson, W. S. B. (1994), *The Physics of Glaciers*, 3rd ed., Elsevier, New York.

Press, W. H., B. P. Flannery, S. A. Teukolsky, and W. T. Vetterling (1993), *Numerical Recipes in FORTRAN 77: The Art of Scientific Computing*, Cambridge Univ. Press, New York.

Raymond, C. F. (1971), Flow in a transverse section of Athabasca Glacier, Alberta, Canada, *J. Glaciol.*, *10*, 55–84.

Sharp, M., J. C. Gemmell, and J. L. Tison (1989), Structure and stability of the former subglacial drainage system of the Glacier de Tsanfleuron, Switzerland, *Earth Surf. Processes Landforms*, *14*(2), 119–134.

Sugiyama, S., G. H. Gudmundsson, and J. Helbing (2003), Numerical investigation of the effects of temporal variations in basal lubrication on englacial strain-rate distribution, *Ann. Glaciol.*, *37*, 49–54.

Thorsteinsson, T., C. F. Raymond, G. H. Gudmundsson, R. A. Bindschadler, P. Vornberger, and I. Joughin (2003), Bed topography and lubrication inferred from surface measurements on fast-flowing ice streams, *J. Glaciol.*, *49*, 481–490.

Tison, J.-L., and B. Hubbard (2000), Ice crystallographic evolution at a temperate glacier: Glacier de Tsanfleuron, Switzerland, in *Deformation of Glacial Materials*, edited by A. J. Maltman, B. Hubbard, and M. J. Hambrey, *Geol. Soc. Spec. Publ.*, *176*, 135–146.

Tison, J. L., and R. D. Lorrain (1987), A mechanism of basal ice-layer formation involving major ice-fabric changes, *J. Glaciol.*, *33*, 47–50.

Truffer, M. (2004), The basal speed of valley glaciers: An inverse approach, *J. Glaciol.*, *50*, 236–242.

Truffer, M., K. A. Echelmeyer, and W. D. Harrison (2001), Implications of till deformation on glacier dynamics, *J. Glaciol.*, *47*(156), 123–134.

Van der Veen, C. J. (1999), *Fundamentals of Glacier Dynamics*, A. A. Balkema, Brookfield, Vt.

Van der Veen, C. J., and I. M. Whillans (1989), Force budget: I. Theory and numerical methods, *J. Glaciol.*, *35*, 53–60.

Vivian, R. (1971), Research in France: Glacier D'Argentiere, *Ice*, *35*, 6–7.

_____

D. M. Chandler and B. P. Hubbard, Centre for Glaciology, Institute of Geography and Earth Sciences, University of Wales, Aberystwyth SY23 3DB, UK. (dic@aber.ac.uk)

A. L. Hubbard and P. W. Nienow, School of Geosciences, University of Edinburgh, Edinburgh EH8 9YL, UK.